Structure of Proton-Conducting Alkali Thio-Hydroxogermanates

Maths Karlsson,*[,†,‡] Aleksandar Matic,[†] Itai Panas,[§] Daniel T. Bowron,[||] Steve W. Martin,[⊥] Carly R. Nelson,[⊥] Chad A. Martindale,[⊥] Andreas Hall,[†] and Lars Börjesson[†]

Department of Applied Physics, Chalmers University of Technology, SE-412 96 Göteborg, Sweden, European Spallation Source Scandinavia, Lund University, SE-221 00 Lund, Sweden, Department of Inorganic Chemistry, Göteborg University, SE-412 96 Göteborg, Sweden, ISIS Facility, CLRC Rutherford-Appleton Laboratory, Chilton, Didcot OX11 0QX, United Kingdom, and Department of Materials Science and Engineering, 2220 Hoover Hall, Iowa State University of Science and Technology, Ames, Iowa 50011

Received March 3, 2008. Revised Manuscript Received July 4, 2008

Using a combination of neutron diffraction, infrared spectroscopy, and first-principles calculations, we have investigated the structure of hydrated and dehydrated proton conducting alkali thio-hydroxogermanates of general formula $M_2GeS_2(OH)_2 \cdot yH_2O$ (M = K, Rb, and Cs). The results show that the structure of hydrated and dry materials are basically the same, which confirms previous indications that the main effect of heating these materials is just a loss of water. We suggest that in the hydrated state the structure of these materials is built of dimers of thio-hydroxogermanate anions, with the water molecules acting as bridges between such dimers. In the dehydrated structure, the thio-hydroxogermanate anions instead form an extended network through the formation of interdimer hydrogen bonds through the −OH groups in the structure. The alkali ions are suggested to act as "space-fillers" in voids formed by the thio-hydroxogermanate anion dimers, in both the hydrated and the dehydrated state.

1. Introduction

Stimulated by the legislative pollution control, the research on environmentally friendly fuel cells, i.e., devices that convert chemical energy into electricity, has intensified since the mid-nineties.[1] One major challenge in this research has been to develop fuel cells operating in the intermediate temperature range 100−500 °C, where no currently available fuel cell performs satisfactorily.[2] In comparison to high-temperature (≥500 °C) fuel cells, the lower temperature increases the endurance of materials and components, keeps the cost fairly low, and allows for a relatively fast start-up.[3] In comparison to low-temperature (≤100 °C) fuel cells, the increased temperature allows for the use of smaller amounts of expensive catalysts because the electrode reactions are faster and gives a wider flexibility in the choice of fuel.[4]

The main factor that limits the development of intermediate temperature fuel cells is the difficulty to develop electrolytes with the required minimum proton conductivity, $\geq 1 \times 10^{-2}$ S cm^{-1}, combined with a high thermodynamic stability.[2] However, recently a new class of high-proton-conducting hydrated thio-hydroxogermanates of general formula $M_xGeS_x(OH)_{4-x} \cdot yH_2O$, where $1 \leq x \leq 4$, $0 \leq y \leq 8$, and M = Na, K, Rb, and Cs, was developed.[5,6] The proton conductivities of these materials reach the required minimum conductivity for temperatures between 100 and 300 °C.[5,6] The unusually high proton conductivities at intermediate temperatures make these materials scientifically interesting and technologically promising for use as electrolytes in future intermediate temperature fuel cells.

Earlier experiments have shown that the alkali thio-hydroxogermanates are amorphous and built of thio-hydroxogermanate anions and alkali ions.[6,7] Moreover, it has been shown by temperature-dependent infrared (IR) spectroscopy that the molecular water can be reversibly removed from the structure by heating to 180 °C and that the materials can be rehydrated by exposure to air for less than 1 h.[8] Details such as the coordination of the thio-hydroxogermanate anions, alkali ions, and water molecules and the influence of the type and concentration of the alkali ions are, however, not yet understood. In particular, it would be interesting to understand how a structure that can be reversibly hydrated and dehydrated is built up.

In this work, we investigate the structure of the alkali thio-hydroxogermanates using neutron diffraction, IR spectroscopy, and first-principles calculations. In a previous study, we have reported on neutron diffraction and IR spectroscopy of $Cs_2GeS_2(OH)_2 \cdot yH_2O$.[7] Now we expand the alkali modification to also include Rb^+ and K^+, whereby the role of

* Corresponding author. E-mail: maths.karlsson@ill.eu.
† Chalmers University of Technology.
‡ Lund University.
§ Göteborg University.
|| CLRC Rutherford-Appleton Laboratory.
⊥ Iowa State University of Science and Technology.

(1) Carette, L.; Friedrich, K. A.; Stimming, U. *ChemPhysChem.* **2000**, *1*, 162.
(2) Steele, B. C. H.; Heinzel, A. *Nature* **2001**, *414*, 345.
(3) Ormerod, R. M. *Chem. Soc. Rev.* **2003**, *32*, 17.
(4) Weber, A.; Ivers-Tiffée, E. *J. Power Sources.* **2004**, *127*, 273.
(5) Poling, S. A.; Nelson, C. R.; Martin, S. W. *Mater. Lett.* **2006**, *60*, 23.
(6) Poling, S. A.; Nelson, C. R.; Martin, S. W. *Chem. Mater.* **2005**, *17*, 1728.
(7) Karlsson, M.; Matic, A.; Nelson, C. R.; Martindal, C. A.; Bowron, D. T.; Martin, S. W.; Börjesson, L. *Solid State Ionics.* **2007**, *178*, 501.
(8) Karlsson, M.; Nelson, C. R.; Martindale, C. A.; Martin, S. W.; Matic, A.; Börjesson, L. *Solid State Ionics.* **2006**, *177*, 1009.

10.1021/cm8006155 CCC: $40.75
Published on Web 09/03/2008

Table 1. Densities of Hydrated and Dehydrated Samples of the Investigated Alkali Thio-Hydroxogermanates

material	bulk density (g/cm^3)	atomic no. density (atoms/$Å^3$)
$Cs_2GeS_2(OD)_2 \cdot 1.1D_2O$	3.440	0.0554
$Cs_2GeS_2(OD)_2$	3.651	0.0451
$Rb_2GeS_2(OD)_2 \cdot 1.1D_2O$	3.008	0.0609
$Rb_2GeS_2(OD)_2$	3.151	0.0497
$K_2GeS_2(OD)_2 \cdot 1.1D_2O$	2.382	0.0646
$K_2GeS_2(OD)_2$	2.464	0.0532

the type of alkali ion can be systematically investigated, and add first-principles calculations to assist the interpretation of the experimental data. By investigating both hydrated (as-prepared) and dehydrated (heated) samples, we aim to elucidate the influence of molecular water on the structure. To decrease the incoherent contribution in the neutron diffractogram, it should be noted that the present experiments were performed on deuterated equivalents.

2. Experimental Section

2.1. Sample Preparation. Samples with three different alkali ions, $K_2GeS_2(OH)_2 \cdot yH_2O$, $Rb_2GeS_2(OH)_2 \cdot yH_2O$, and $Cs_2GeS_2(OH)_2 \cdot yH_2O$, were prepared by mixing aqueous solutions containing stoichiometric amounts of the alkali hydrosulfide MSH (M = K, Rb, and Cs) and commercial quartz-type GeO_2. Subsequently the excess water was evaporated at ~75 °C for a period over a week. The samples were finally vacuum-dried at room temperature overnight and stored in an inert atmosphere. Ideally, the corresponding reaction for the synthesis of these materials is written as

$$2MSH + GeO_2 + yH_2O \rightarrow M_2GeS_2(OH)_2 \cdot yH_2O \quad (1)$$

Here, $y \approx 0.2-0.6$ for M = Cs, $y \approx 0.8$ for M = Rb, and $y \approx 0.4-0.8$ for M = K are reported estimations made on the basis of thermal gravimetric analysis (TGA).[6] The deuterated equivalents were obtained in the same way but using MSD (M = K, Rb, and Cs) and D_2O instead of MSH and H_2O, respectively. Dehydrated samples were prepared by heating the as-prepared samples at 180 °C in a vacuum for approximately 2 h. By measuring the weight change during this procedure, we determined y to be 1.1 in each of the hydrated materials. The discrepancy between our value of y and that reported earlier based on TGA may be a consequence of reproducibility since the two experiments were performed on samples from different batches. Densities were measured with the use of a gas micropycnometer and are reported in Table 1. Further details of the sample preparation procedure can be found elsewhere.[6]

2.2. Neutron Diffraction. The neutron diffraction experiments were performed at the SANDALS time-of-flight diffractometer at the pulsed neutron source ISIS, Rutherford Appleton Laboratory, United Kingdom. The SANDALS diffractometer, described in detail in ref 9, receives neutrons with wavelengths from 0.05 to 5 Å. The 660 detectors are summed into 18 groups which cover an angular range of 3.8−39°, yielding scattering vectors (Q) in the range $0.1-50$ $Å^{-1}$. Note that because of an absorption resonance of the Cs atoms, which caused odd features in the measured diffractogram at high Q-values, we used only the $0.1-27$ $Å^{-1}$ range for the Cs-based material.

The samples were ground into fine powders using an agate mortar and a pestle, and loaded in flat sample cells of a 68% titanium and 32% zirconium alloy, which does not contribute to any coherent scattering. The sample thickness was 2 mm and the beam at the sample was circular with a diameter of 32 mm. For each sample, the measuring time was approximately 12 h. All measurements were performed at room temperature. A measurement of the empty sample container was performed in order to correct for the background, and a measurement of a vanadium-standard was carried out in order to correct for the detector efficiency and normalize the data onto an absolute scale of barns per steradian per atom. Using the on-site GUDRUN software, which incorporates the ATLAS routines,[10,11] the raw data were corrected for multiple scattering, absorption, inelasticity effects, and finally merged to obtain the total neutron static structure factor $S(Q)$. The correction procedure was performed by using $y = 1.1$ for the hydrated samples and $y = 0$ for the dehydrated samples, respectively. The levels of the measured differential neutron scattering cross-sections, which are related to the $S(Q)$s, were well within the range of expected values.

$S(Q)$ is related to the total pair-correlation function $G(r)$ by a Fourier transformation according to

$$G(r) = 1 + \frac{\sum_{i=1}^{n} c_i \bar{b}_i^2}{\left(\sum_{i=1}^{n} c_i \bar{b}_i\right)^2} \frac{1}{2\pi^2 \rho_0 r} \int_0^\infty [S(Q) - 1] \sin(Qr) Q \, dQ \quad (2)$$

In practice, the integration range in eq 2 is limited to the Q-range offered by the instrument, which causes truncation errors in the pair-correlation function. To suppress such features, the integrand is generally multiplied by a suitable modification function $w(Q)$.[12] In our analysis, the function applied was

$$w(Q) = \begin{cases} 1 - 3Z^2 & : \quad Q < Q_m/3 \\ \frac{3}{2}(1 - 2Z + Z^2) & : \quad Q_m/3 < Q < Q_m \\ 0 & : \quad Q > Q_m \end{cases} \quad (3)$$

where Q_m is the largest Q-value and $Z = Q/Q_m$.

2.3. Infrared Spectroscopy. The far-IR spectra, $50 - 500$ cm^{-1}, were measured using a Bruker IFS 66v/s FT-IR spectrometer equipped with a deuterated triglycerine sulfate (DTGS) detector and a Mylar 6/Ge beam splitter. The spectra were obtained by averaging more than 500 scans. The experiments were performed in a vacuum at room temperature in a transmittance setup with the samples dispersed to 5 wt % in pellets of 0.1 g of polyethylene. The circular pellets (Ø13 mm) were obtained by applying a pressure of 7 tons to the mixtures. All sample preparations except the pellet pressing and the loading of the samples into the spectrometer, processes that took approximately 1 min each, were carried out in an inert atmosphere.

2.4. First-Principles Calculations. Because the static structure factor of the alkali thio-hydroxogermanates has contributions from 15 partial pair-correlation functions, a direct interpretation of the neutron diffraction data and the disentanglement of the different contributions to the experimental $G(r)$ is very difficult. Thus, we have performed first-principles calculations of model structures of the cesium thio-hydroxogermanate to assist the interpretation of the experimental data and test structural models. We model the glass structure with a configuration, derived from a crystalline

(9) Benmore C.; Soper A. *The SANDALS Manual*; ISIS Facility, Rutherford Appleton Laboratory: Didcot, U.K., 1998.
(10) Hannon A. C.; Howells W. S.; Soper A. K. In *Second Workshop on Neutron Scattering Data Analysis (WONSDA)*, March 14−16, 1990; Institute of Physics Conference Series; Adam Hilger: Bristol, U. K., 1990; Vol. 107.
(11) Soper, A. K.; Howells, W. S.; Hannon, A. C. *ATLAS Analysis of Time-of-Flight Diffraction Data from Liquid and Amorphous Samples, version 2.0 Incorporating the SANDALS Survival Guide*; ISIS Facility, Rutherford Appleton Laboratory: Didcot, U.K., 2000.
(12) Waser, J.; Schomaker, V. *Rev. Mod. Phys.* **1953**, *25*, 671.

analog, but fully relaxed to match with the same stoichiometry and density as the Cs-based thio-hydroxogermanate in the experiment. With this procedure we obtain a structural model where the short-range order can be analyzed and compared to the experimental results.

A candidate three-dimensional structure was generated by taking the orthorhombic crystal structure of $Na_2GeS_2(OH)_2 \cdot 5H_2O$ as the starting point.[13] This structure includes 8 formula units, i.e., 16 Na ions, 8 thio-hydroxogermanate anions, and 40 water molecules in the unit cell. In the present study, the Na ions were replaced by Cs ions and the number of water molecules was reduced to one per formula unit to be in agreement with the composition in the experiment. Thus, in all, 96 atoms were subject to full geometry optimization by employing first-principles density functional theory. Only the γ-point was considered in the periodic boundary condition calculations. Justifications for this approximation to model the glass are as follows: (a) negligible influence of dispersion of bands, (b) the optimized structure of the eight symmetry-independent germanates in the unit cell is suggested to model well the short-range order in the corresponding glass, and (c) periodic boundary conditions were employed in order to provide a reasonable embedding to the Cs germanate hydrate cluster. The DMOL3 program package[14] as implemented in Materials Studio[15] was employed. The BLYP GGA functional[16,17] was used in the geometry optimization in conjunction with a numerical double-ζ basis set, and DSPP semicore pseudopotentials on Ge, S, and Cs. The structure was deemed to be converged when a maximum energy gradient less than 1×10^{-5} Ha/A was reached.

From the generated structure we have calculated the partial radial pair-correlation functions at the discrete points $r_i = (i + 1/2)\Delta r$ as

$$g_{AB}(r_i) = \frac{1}{\rho_B} \frac{\langle h_{AB}(i) \rangle_A}{4\pi r_i^2 \Delta r} \quad i = 1, 2, 3, \ldots \tag{4}$$

where ρ_B is the average number density of B, $h_{AB}(i)$ is the number of B atoms in the spherical shell $[i\Delta r, (1 + i)\Delta r]$ surrounding A atoms, and the average is taken over all unique A atoms in the model. The total neutron-weighted pair-correlation function is then given by

$$G_{calc}(r_i) = \frac{\sum_{A,B} \rho_A \rho_B \overline{b_A}\ \overline{b_B} g_{AB}(r_i)}{\left(\sum_A \rho_A \overline{b_A}\right)^2} \tag{5}$$

The sampling interval for calculating $G(r)$ was set to $\Delta r = 0.1$ Å.

3. Results

3.1. Neutron Diffraction and First-Principles Calculations. Figure 1 shows the static structure factors of hydrated and dehydrated samples of $Cs_2GeS_2(OD)_2 \cdot yD_2O$, $Rb_2GeS_2(OD)_2 \cdot yD_2O$ and $K_2GeS_2(OD)_2 \cdot yD_2O$ obtained from the neutron diffraction experiments. For the high Q-range, ≥ 6 Å^{-1}, cf. Figure 1(a), the structure factors of the six different materials are overall largely the same, indicating only minor differences in the short-range structures of these materials. In particular, we note that

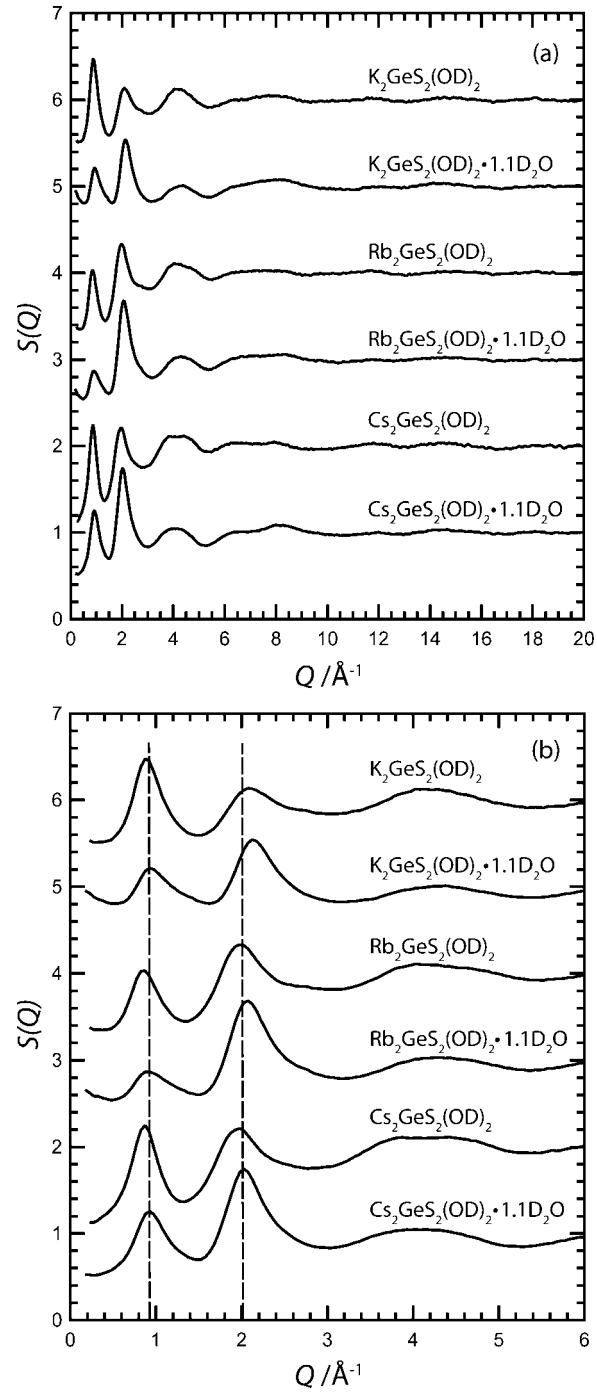

Figure 1. Experimental neutron static structure factors of hydrated and dehydrated samples of $Cs_2GeS_2(OD)_2 \cdot yD_2O$ $Rb_2GeS_2(OD)_2 \cdot yD_2O$, and $K_2GeS_2(OD)_2 \cdot yD_2O$: (a) Q-range 0.2−20 Å^{-1}, (b) expansion of the 0.2−6 Å^{-1} range. For clarity, the diffractograms have been vertically shifted by unity. The two vertical lines serve as guidance.

the structure factor of each material oscillates around 1 at high Q-values, which shows that they are properly corrected and normalized. In the low Q-range, which is expanded in Figure 1b, we can observe some significant differences among the different compositions. The most pronounced difference regards the position and intensity of the first two peaks, centered at ~0.9 and at ~2 Å^{-1}, respectively; see Table 2 for more exact values. For the hydrated materials, the first peak is centered at the same Q-value for the Cs- and K-based materials, whereas for

(13) Krebs, B.; Wallstab, H. J. *Inorg. Chim. Acta* **1981**, *54*, L123.
(14) Delley, B. *J. Chem. Phys.* **1990**, *92*, 508.
(15) *Materials Studio, DMol3*, version 2.2; Accelrys Inc.: San Diego, 2007; www.accelrys.com.
(16) Becke, A. D. *Phys. Rev. A.* **1988**, *38*, 3098.
(17) Lee, C. T.; Yang, W. T.; Parr, R. G. *Phys. Rev. B* **1988**, *37*, 785.

Table 2. Peak Positions for the First Two Peaks in $S(Q)$, and for the First Three Strong Peaks in $G(r)$, for Hydrated and Dehydrated Samples of $Cs_2GeS_2(OD)_2 \cdot yD_2O$, $Rb_2GeS_2(OD)_2 \cdot yD_2O$, and $K_2GeS_2(OD)_2 \cdot yD_2O$[a]

material	Q_1 (Å^{-1})	Q_2 (Å^{-1})	r_1 (Å)	r_2 (Å)	r_3 (Å)
$Cs_2GeS_2(OD)_2 \cdot 1.1D_2O$	0.93	2.03	0.95	1.79	2.22
$Cs_2GeS_2(OD)_2$	0.88	1.98	0.79(n)/1.04	1.82	2.16
$Rb_2GeS_2(OD)_2 \cdot 1.1D_2O$	0.90	2.07	0.98	1.80	2.18
$Rb_2GeS_2(OD)_2$	0.85	1.98	0.98	1.81	2.16
$K_2GeS_2(OD)_2 \cdot 1.1D_2O$	0.93	2.13	0.99	1.79	2.23
$K_2GeS_2(OD)_2$	0.88	2.10	0.98	1.82	2.17

[a] (n) refers to a negative peak, see text. The uncertainties for the peak positions in $S(Q)$ and $G(r)$ are ±0.02 and ±0.01, respectively.

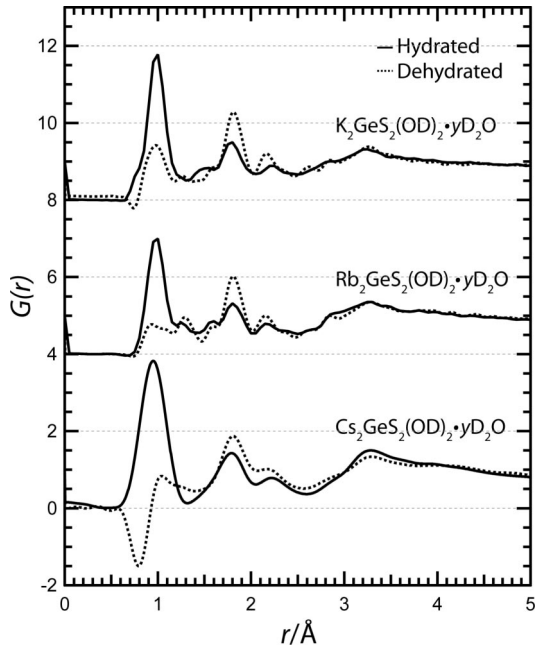

Figure 2. Neutron pair-correlation functions $G(r)$ for hydrated and dehydrated samples of $Cs_2GeS_2(OD)_2 \cdot yD_2O$, $Rb_2GeS_2(OD)_2 \cdot yD_2O$, and $K_2GeS_2(OD)_2 \cdot yD_2O$. For clarity, the pair-correlation functions have been vertically offset by 4.

the Rb-based equivalent, it is slightly down-shifted. The second peak shifts toward lower Q-values as the ionic radius of the alkali ion increases. Upon dehydration, both the first and the second diffraction peak shifts toward lower Q-values and decreases in intensity, and the first peak in particular sharpens.

Figure 2 shows the pair-correlation functions, $G(r)$, for both the hydrated and the dehydrated materials, as obtained from the structure factors. Figure 3 shows the pair-correlation function for the calculated structures, $G_{calc}(r)$, for both the small and the large computational box, together with the experimental pair-correlation function, $G(r)$, of the hydrated and dehydrated Cs-based material. Table 3 shows the positions and intensities of the strongest peaks in the partial pair-correlation functions, obtained from these calculations. As seen in Figure 3, there is overall a good agreement between the experimental and calculated pair-correlation functions in the range $r = 0-5$ Å, apart from the peak at 2.5 Å, which is much more pronounced in the calculated structures and the region around 1 Å for the dehydrated material, as discussed further below. The calculated pair-correlation functions have of course much sharper peaks as

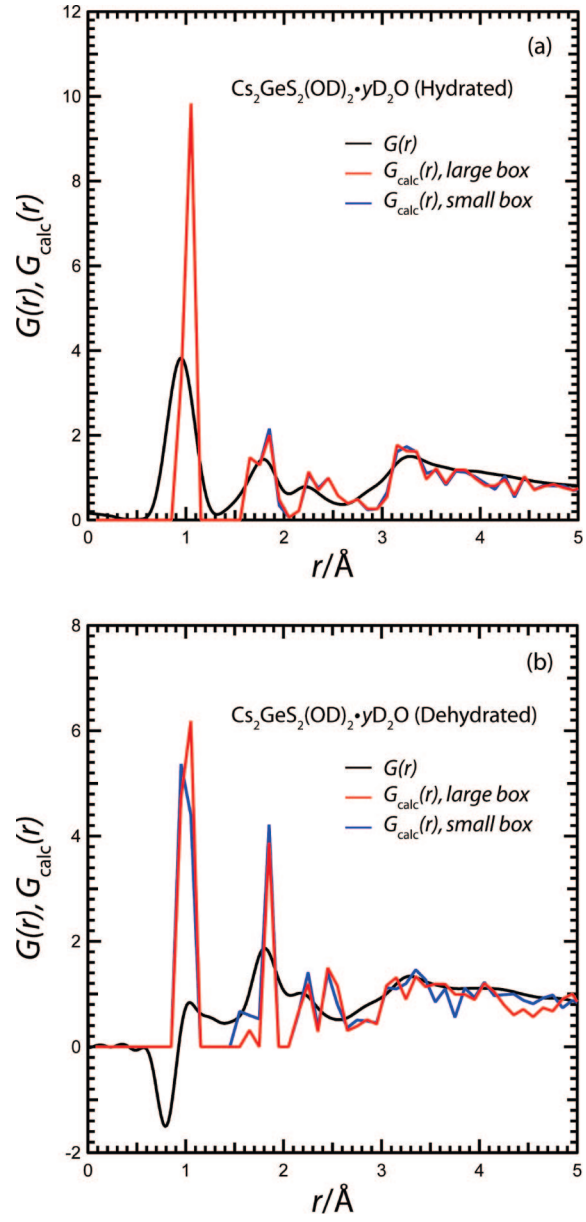

Figure 3. Comparison between the experimental and calculated total pair-correlation function for (a) hydrated and (b) dehydrated $Cs_2GeS_2(OD)_2 \cdot yD_2O$.

they do not contain any contributions from thermal broadening or instrumental resolution. The calculated model can also be expected to be more ordered than the real material as it is derived from a crystalline starting configuration. Morevoer, we see in Figure 3 that there are only minor differences between the calculated pair-correlation functions for the small and large computational box, for both the hydrated and the dehydrated materials. This shows that the contribution from second-nearest thio-hydroxogermanate anions to $G_{calc}(r)$ is small and the contribution from third-nearest thio-hydroxogermanate anions is negligible. This justifies the possible use of first-principles periodic boundary condition calculations in conjunction with sufficiently large unit cells for extracting local signatures of glasses.

Considering first the hydrated materials in Figure 2, the strongest features in $G(r)$ are three distinct peaks at ~1, ~1.8, and ~2.2 Å, respectively, and a broader peak centered at

Table 3. Interatomic Distances (r) and Peak Intensities (I) of the Strongest Peaks in the Partial Pair-Correlation Functions $G_{ij,\mathrm{calc}}(r)$ as Calculated from the Generated Structure[a]

$G_{ij,\mathrm{calc}}(r)$	r (Å)	I_d (arb. units)	I_h (arb. units)
Ge−Ge	∼5, ≥6 (∼4.5, ≥ 6 hydr.)	1.5, 2	1.5, 1.5
Ge−S	2.2	60	70
Ge−O	1.9, ∼4	115, 10	130, 15
Ge−Cs	≥4	14	10
Ge−H	2.4, ≥3	44, 32	60, 30
Cs−Cs	∼4	5	3
Cs−H	≥3	21	17
Cs−O	∼3	25	23
Cs−S	∼3.5	18	8
O−H	1, 1.7, 3.2	450, 15, 10	1050, 55, 40
O−S	3.3	20	20
O−O	2.7	10	14
S−S	3.8	2	1
S−H	≥2.2	12	4
H−H	1.7, ∼2	0, 5	30, 18

[a] The subscripts d and h refer to the dehydrated and hydrated structure, respectively.

around 3.3 Å. The first peak is assigned to O−D correlations because no other interatomic distance is this short in these materials. This assignment is also in agreement with the O−D distance of $r_{\mathrm{O(II)-D(I)}} = 0.97$ Å, estimated by adding the respective ionic radii. Here, and in the following in this paper, we have taken the ionic radii from Shannon,[18] whereas the numbers within the parentheses refer to the nominal coordination numbers. Also based on the sum of the ionic radii, we have estimated Ge−O and Ge−S correlations to be located at around $r_{\mathrm{Ge(IV)-O(II)}} = 1.74$ Å and $r_{\mathrm{Ge(IV)-S(VI)}} = 2.23$ Å, which agrees well with the peaks located at ∼1.8 and ∼2.2 Å. Further support for these assignments is obtained from the interatomic distances and intensities for the calculated Cs-based structure, see Figure 3 and Table 3. Moreover, we assign the broad peak centered at around 3.3 Å in Figure 2 to O−S correlations and different correlations involving the alkali ions, also based on the distances and intensities given in Table 3. In particular, we note that the shoulders on the low and high r-flank of this peak likely originate from M−O and M−S (M = K, Rb, and Cs) correlations, respectively. Depending on the coordination number and type of alkali ion, these correlations are expected at slightly different distances in respective pair-correlation functions. Specifically, K−O and K−S correlations are expected at 2.7−3.0 and 3.2−3.5 Å, respectively, Rb−O and Rb−S correlations at 2.9−3.2 and 3.4−3.6 Å, respectively, and Cs−O and Cs−S distances at 3.0−3.2 and 3.5−3.7 Å, respectively. Obviously, M−O and M−S correlations are expected to shift to higher r-values with the alkali ionic radius, and as seen in Figure 2, this is indeed the case for the two shoulders of the broad 3.3 Å peak. Additional peaks are found for the Rb- and K-based materials at ∼1.2 and ∼1.6 Å. The 1.6 Å peak is most likely related to D−D correlations of water molecules, which agrees well with the D−D distance of $r_{\mathrm{D(I)-D(I)}} = 1.55$ Å, estimated by using a O−D distance of 0.97 Å and a D−O−D bond angle of 104.5°.[19] This is also supported by the distance of the H−H correlations for the calculated structure, 1.7 Å, see Table 3. The 1.2 Å peak is more difficult to assign. Based on the ionic radii this peak could be related to M−D correlations but since the Cs−H correlations in the calculated structure is found at ≥3 Å, this seems very unlikely. It could also come from an impurity. Regarding the Cs-based material, the 1.2 Å and 1.6 Å peaks are likely concealed by the broader nature of the O−D and Ge−O correlation peaks due to the slightly lower resolution as a result of a smaller Q-range.

Upon dehydration, the main effect on the pair-correlation function is a substantial drop in intensity of the O−D correlation peak, a result of significantly less deuterons in the dehydrated samples. For the Cs-based material, we observe that the low r-flank of the O−D peak becomes negative after dehydration. This may be a consequence of some residual hydrogen in the sample as the scattering length of hydrogen is negative, resulting in a negative peak in $G(r)$. However, this negative peak is located at an unphysical short distance of about 0.79 Å, see Table 2. This feature points toward that this peak results from odd features in $S(Q)$ due to the absorption resonance of the Cs atom (as was noted above) even though it has been truncated. The actual intensity expected for the O−D peak can be estimated from the calculated pair-correlation function in Figure 3b. Furthermore, we observe that the ∼1.8 Å peak, related to mainly Ge−O correlations, shifts to larger r-values and increases in intensity, and the ∼2.2 Å peak, related to mainly Ge−S correlations, becomes down-shifted for each material, see Table 2. For the other peaks in the pair-correlation functions, neither any significant intensity changes nor peak shifts can be observed upon dehydration.

One can note that in the calculated pair-correlation function the peak at 2.4 Å is more pronounced than for the real material. This peak originates from the Ge−H correlation, see Table 3, which is the only correlation in the range 2.2−2.7 Å. The reason for this discrepancy may be traced to some residual hydrogen found in the Cs-based sample, as discussed above. The residual hydrogen will decrease the intensity of the Ge−H correlation because of the negative scattering length of hydrogen.

3.2. Infrared Spectroscopy. Figure 4 shows the far-IR (50−350 cm^{-1}) spectra of hydrated and dehydrated samples of the investigated alkali thio-hydroxogermanates. As the intramolecular vibrations in water molecules have frequencies higher than 500 cm^{-1},[20] we can expect that this part of the spectrum is solely related to vibrations of the thio-hydroxogermanates and charge-balancing alkali ions.

Our first observation in Figure 4 is that the spectra of hydrated and dehydrated samples look essentially the same. For each material we find distinct bands at around 185, 220, 270, and 340 cm^{-1}, whereas a broad band is centered between 92 and 135 cm^{-1}. The position of the lowest-frequency band is evidently substantially dependent upon the type of alkali ion. Figure 5 shows the peak frequency dependence of this band on the inverse of the square root of the alkali ion mass, $M_\mathrm{c}^{-1/2}$. The almost linear relationship suggests that this band is related to vibrations of the alkali ions, and that the alkali ions vibrate against a rigid anionic surrounding. However, one should here note that the shape

(18) Shannon, R. D. *Acta Crystallogr., Sect. A* **1976**, *32*, 751.
(19) Wilson, S.; Gerratt, J. *Mol. Phys.* **1975**, *30*, 789.
(20) Marechal, Y. *J. Chem. Phys.* **1991**, *95*, 5565.

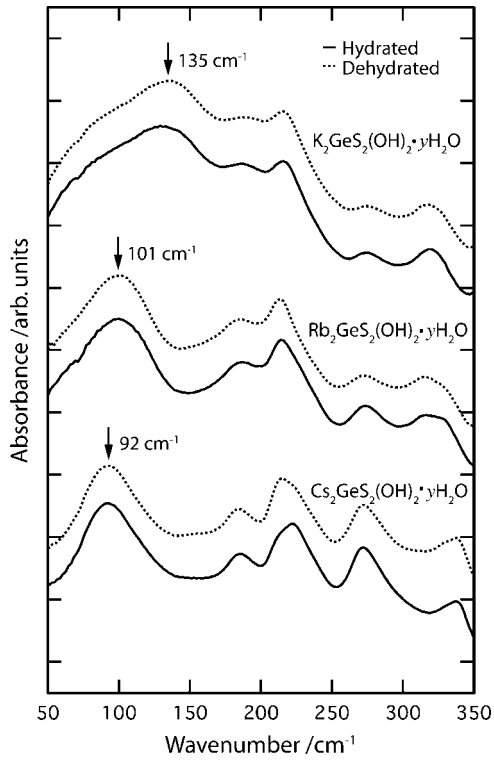

Figure 4. Far-IR spectra of hydrated and dehydrated samples of $Cs_2GeS_2(OH)_2 \cdot yH_2O$, $Rb_2GeS_2(OH)_2 \cdot yH_2O$ and $K_2GeS_2(OH)_2 \cdot yH_2O$. The spectra have been baseline corrected and vertically offset for clarity.

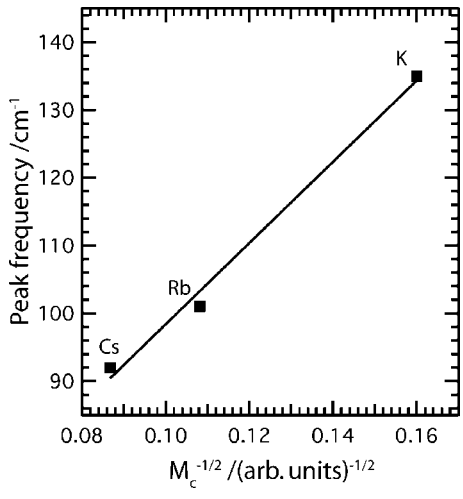

Figure 5. Peak frequency dependence of the alkali ion band versus the inverse of the square root of the corresponding alkali ion mass $M_c^{-1/2}$. The linear line represents a least-squares fit to the data, whereas the error bars of the peak frequencies are within the size of the symbols.

of this band changes significantly with the type of alkali ion. In particular, we can for the K-based material observe a distinct shoulder of this band, located at around 70 cm^{-1}. For the Rb-based material only an indication of a shoulder is observed in the asymmetric band profile, but just at the limit of our frequency window, whereas the band is quite symmetric for the Cs-based material. This low frequency shoulder may be associated to a "secondary" site for the alkali ions in the structure. The dependence of this low frequency contribution on the cation mass cannot be determined as it moves outside of our spectrum for the Rb- and Cs-based materials. The other bands in the spectra between 150 and 350 cm^{-1} are most likely related to different types of vibrations of the thio-hydroxogermanate anions. This is strengthened by the fact that their frequencies are basically the same independent of the type of alkali ion.

4. Discussion

By combining the results obtained from neutron diffraction, infrared spectroscopy and first-principles calculations we are now able to reveal several important structural characteristics of proton-conducting alkali thio-hydroxogermanates. As shown in Figures 1, 2 and 4, there is a remarkable similarity between the structure factors, pair-correlation functions, and infrared spectra of hydrated and dehydrated samples. This confirms previous indications that the main effect of heating the hydrated materials is just a loss of molecular water, i.e., neither any phase transitions nor structural degradations occur in the temperature range of 25−300 °C.[7,8] This suggests that the structures of the hydrated and dehydrated materials are, apart from the presence of water molecules in the hydrated ones, basically the same.

A direct interpretation of the diffraction peaks into real space is in general difficult since this conversion involves a Fourier transformation. However, the first sharp diffraction peak (FSDP), located at Q_1, can for amorphous materials be related to an intermediate-range order with a characteristic length scale of about $2\pi/Q_1$.[21] In our case, this corresponds to a distance of 7 Å. The intensity increase and sharpening of the FSDP upon dehydration, observed for all materials, can be related to an increased density contrast as the water molecules are removed from the structure. Moreover, the fact that the position of the two first diffraction peaks slightly decreases upon dehydration suggests that the characteristic length scale in the structure increases as water is removed, i.e., the structure expands. This could be a result of the water molecules acting as a dielectric medium that decreases the repulsive interactions between the negatively charged thio-hydroxogermanate ions and between the positively charged alkali ions. Speculatively, we note that for the second diffraction peak, which is located at Q_2, $2\pi/Q_2$ corresponds to ∼3 Å in real space, which suggests that this peak is related to M−O and M−S distances, as estimated from both the ionic radii and the Cs−O and Cs−S distances and intensities in the calculated structure, see Table 3. This is also in agreement with the downshift of this peak with increasing size of the alkali ion, as this will naturally move the thio-hydroxogermanate and alkali ion farther apart. It should here be said that the alkali ions in all likelihood tend to coordinate to the negatively charged sulfurs of the thio-hydroxogermanates. One should note, however, that the position and shape of the peaks in the $S(Q)$ for a multicomponent system has contributions from a number of partial structure factors. Thus, the shift of the FSDP and also for the second peak upon dehydration may partially be due to that the different contributing pair-correlation functions change in intensity, even though the underlaying structure remains unchanged.

That the alkali ions are to a much lesser extent coordinated to the molecular water is inferred by our IR spectroscopy

(21) Elliot, S. R. *Phys. Rev. Lett.* **1991**, *65*, 711.

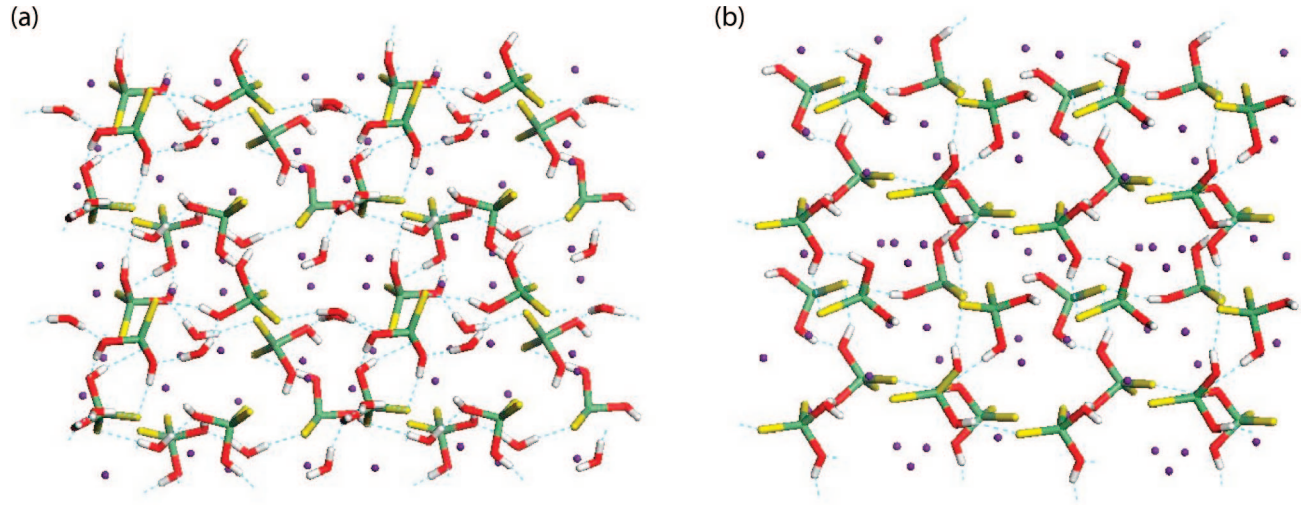

Figure 6. Configurations of the calculated (a) hydrated and (b) dehydrated structure. The oxygens are labeled with red, the sulfurs with yellow, the hydrogens with white, and the cesium and germanium ions with violet and green, respectively. The dashed lines are hydrogen bonds.

results (Figure 4). The alkali ion band is unaffected by dehydration, implying that the local coordination of the alkali ions does not change significantly with water content. If the alkali ions were mainly coordinated to the molecular water, their vibrations would certainly change, which should be manifested as a clear frequency shift and/or change in shape of the corresponding band in the spectrum. In addition, the fact that the alkali ions vibrate against a rigid environment, as evidenced by the linear relationship between the frequency of the alkali ion vibrations and the inverse of the alkali ion mass, provides further support for that the alkali ions are not surrounded by the lighter water molecules in the first coordination shell. The fact that the alkali ion band becomes narrower with increasing size of the alkali ion suggests a more well-defined environment of the alkali ions the larger they are. This can be understood from the fact that a large alkali ion has a higher coordination number and thus cannot adopt as many local configurations as a smaller one.

By comparing the IR spectra of the alkali thio-hydroxogermanates to the reported IR spectra of $0.20R_2O$-$0.80GeO_2$ (R = K, Rb and Cs)[22] glasses, we find a remarkable agreement. For these glasses, two well separated bands, related to vibrations of alkali ions in two different sites, were found.[22] Specifically, for the Cs, Rb, and K germanate glasses, these bands are located at 80 and 37 cm^{-1}, 100 and 46 cm^{-1}, and 135 and 67 cm^{-1}, respectively.[22] Here, the high-frequency band was assigned to a site similar to that in the corresponding crystal while the low-frequency band was ascribed to a "secondary" site of higher energy and whose coordination number and charge density are different from their optimum values.[22] The agreement between the high-frequency bands of the Rb and K germanate glasses and the alkali ion bands for the corresponding thio-hydroxogermanates is excellent, whereas for the Cs-based material, the agreement is worse, compare 80 to 92 cm^{-1}. Furthermore,

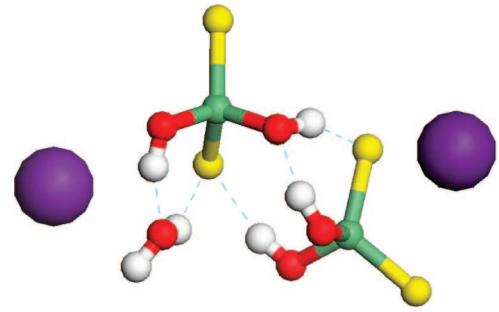

Figure 7. Configuration of the local structure of $Cs_2GeS_2(OH)_2 \cdot 1H_2O$ as obtained from the first-principles calculations. The oxygens are labeled with red, the sulfurs with yellow, the hydrogens with white, and the cesium and germanium ions with violet and green, respectively. The dashed lines are hydrogen bonds.

we note that the frequency of the low-frequency shoulder of the K-based thio-hydroxogermanate at 70 cm^{-1} (cf. Figure 4) compares well to the low-frequency K vibration in the germanate glass at 67 cm^{-1}, which supports the presence of an additional "secondary" site for the alkali ions also in the thio-hydroxogermanate structure. For the Rb- and Cs-based counterparts, we are limited by the experimental range of the spectrometer to reach low enough wavenumbers but the highly asymmetric shape of the alkali ion band in the Rb-based thio-hydroxogermanate most likely is a signature of this band.

To get a more detailed idea of how the structure of the investigated alkali thio-hydroxogermanates may look like, we consider configurations of the calculated hydrated and dehydrated structures. Figure 6 shows a general view of the two structures, and Figure 7 shows a local configuration in the hydrated material. From Figures 6a and 7, we see that the hydrated structure is built up of dimers of thio-hydroxogermanate anions, which are hydrogen bound to each other and that water molecules act as bridges between such dimers. In the dehydrated structure (cf. Figure 6b) we instead have a percolating network of thio-hydroxogermanate anions connected through hydrogen bonds. That is, the role of the water molecules is to break the hydrogen bonds between neighboring thio-hydroxogermanate anion dimers to form dimers which are only connected to each other via water

(22) Kamitsos, E. I.; Yiannopoulos, Y. D.; Jain, H.; Huang, W. C. *Phys. Rev. B* **1996**, *54*, 9775.
(23) Kreuer, K. D.; Weppner, W.; Rabenau, Q. *Solid State Ionics.* **1981**, *3−4*, 353.
(24) Kreuer, K. D. *Chem. Mater.* **1996**, *8*, 610.

molecules. It should be noted that it has previously been proposed that the molecular water in alkali thio-hydroxogermanates is confined to cages built up of the thio-hydroxogermanate anions and the alkali ions,[7] but from the present work this seems not to be the case. Furthermore, we see that the Cs ions act as "space-fillers" in "voids" formed by the thio-hydroxogermanate dimers. The fact that the Cs ions are found in a surrounding of heavy thio-hydroxogermanates rather than being coordinated to water molecules agrees well with the linear relationship between the frequency of the alkali ion vibration and the inverse of the alkali ion mass as well as with the very similar IR spectra of hydrated and dehydrated materials, as discussed above. From the calculated structure, we can also get an idea of the intermediate range order in the structure. The characteristic length scale, about 7 Å, as revealed by the FSDP, corresponds well with the interdimer separation for both the calculated hydrated and the calculated dehydrated structure. However, the FSDP is, most likely, not solely related to interdimer separations but also to intradimer Ge−Ge correlations, which are separated by approximately 5 Å. This suggestion is based on the fact that the separation between intradimer thio-hydroxogermanate anions increases when the water is removed, as reflected by the Ge−Ge distances given in Table 3, which is in agreement with the simultaneous down-shift of the FSDP.

The agreement between the short-range order derived from the first-principles calculations and the experimental results suggests that the structure of alkali thio-hydroxogermanates of hydrated and dehydrated materials is given, at least reasonably well, by the calculated structures shown in Figure 6. However, to obtain a complete picture of the structure built up of hydrogen bound dimers of thio-hydroxogermanate anions and space filling alkali ions, and to clarify the effect of type of alkali ion, more investigations by, for example, reverse Monte Carlo simulations, would be beneficial.

The insight into the structure of the investigated materials also provides some ideas regarding the proton transport in this new class of materials. It has previously been shown that the hydrated materials display a remarkably higher conductivity than the dehydrated ones.[6] The higher conductivity in the hydrated state is most likely related to the larger number of sites for the protons in the structure because of the intercalated water molecules, whereas in the dehydrated state the protons are possibly "trapped" in the thio-hydroxogermanate dimers. A second reason for the large difference in conductivity is that the "free" dimers of thio-hydroxogermanate anions in the hydrated state are likely to be more flexible, i.e., to move more easily through, for instance, rotations, than the reasonably stiffer nature of the extended network of thio-hydroxogermanate dimers in the dehydrated state. The presence of other dynamical processes than just proton jumps that govern the proton transport in the hydrated state is supported by the non-Arrhenius behavior of the conductivity.[6]

5. Conclusions

We have investigated the structure of the proton conducting alkali thio-hydroxogermanates $M_2GeS_2(OH)_2 \cdot yH_2O$ (M = K, Rb, and Cs), using a combination of neutron diffraction, infrared spectroscopy and first-principles calculations. The results show that the structure of hydrated and dry materials are basically the same, which confirms previous indications that the main effect of heating these materials is just a loss of molecular water, i.e., neither any phase transitions nor any structural degradations occur in the temperature range of 25−300 °C. Comparison of the experimental results with first-principles calculations suggests that in the hydrated state the structure of these materials is built up of dimers of thio-hydroxogermanate anions, and that the water molecules act as bridges between such dimers. In the dehydrated structure, the thio-hydroxogermanate anions instead form an extended network through the formation of interdimer hydrogen bonds, whereas the alkali ions are suggested to act as "space-fillers" in "voids" formed by the thio-hydroxogermanate anion dimers, in both the hydrated and the dehydrated structure.

Acknowledgment. This work was financially supported by the National Graduate School in Materials Science in Sweden and the Swedish Research Council, and the United States Department of Energy's Hydrogen Program under Cooperative Agreement DE-FC36-00GO1-531. Allocated beam time at the SANDALS diffractometer at the ISIS Pulsed Neutron and Muon Source is gratefully acknowledged.

Note Added after ASAP Publication. Due to a production error this paper published ASAP September 3, 2008 displaying an incomplete image of Figure 6; the corrected version published ASAP September 6, 2008.

CM8006155